LA-UR:04-6267

Direct observation of the formation of polar nanoregions in $Pb(Mg_{1/3}Nb_{2/3})O_3$ using neutron pair distribution function analysis

I.-K. Jeong,* T. W. Darling, J. K. Lee, Th. Proffen, and R. H. Heffner
Los Alamos National Laboratory, Los Alamos, NM 87545, USA.

J. S. Park and K. S. Hong
School of Materials Science and Engineering, Seoul National Univ., Seoul, Korea.

W. Dmowski
Department of Materials Science and Engineering, Univ. Tennessee, Knoxville, TN 37996, USA

T. Egami
Department of Materials Science and Engineering and Department of Physics and Astronomy, Univ. Tennessee, Knoxville, TN 37996 and Oak Ridge National Laboratory, Oak Ridge, TN, 37831, USA

Using neutron pair distribution function (PDF) analysis over the temperature range from 1000 K to 15 K, we demonstrate the existence of local polarization and the formation of medium-range, polar nanoregions (PNRs) with local rhombohedral order in a prototypical relaxor ferroelectric $Pb(Mg_{1/3}Nb_{2/3})O_3$. We estimate the volume fraction of the PNRs as a function of temperature and show that this fraction steadily increases from 0 % to a maximum of $\sim$ 30% as the temperature decreases from 650 K to 15 K. Below T$\sim$200 K the PNRs start to overlap as their volume fraction reaches the percolation threshold. We propose that percolating PNRs and their concomitant overlap play a significant role in the relaxor behavior of $Pb(Mg_{1/3}Nb_{2/3})O_3$.

PACS numbers: 77.84.Dy, 61.43.Gt, 64.70.Kb, 61.12.Ld

Relaxor ferroelectrics, such as lead magnesium niobate $Pb(Mg_{1/3}Nb_{2/3})O_3$ (PMN), have been widely applied due to their high, relatively temperature-independent, permittivities. Relaxors are characterized by a frequency dispersion in their maximum permittivity temperature (T_M $\sim$285 K in PMN), with no macroscopic phase transition into a ferroelectric state at T_M [1]. These behaviors are fundamentally different from those of normal ferroelectrics and are similar to spin-glasses [2]. It is now believed that local polarization, resulting from structural and chemical disorder, plays a crucial role in relaxor behavior [3, 4]. Several models have been proposed to explain the nature of the interactions between these local polarizations and the mechanism for relaxor behavior [3, 5, 6, 7, 8]. These models include superparaelectric [3, 5] and dipole glasses [6], as well as random field interactions [7]. The microscopic mechanism behind relaxor ferroelectricity is, however, not fully understood, and is still controversial due to its high degree of complexity.

In this Letter, we report the temperature evolution of the local and medium-range crystal structure of PMN from 1000 K to 15 K using neutron pair distribution function (PDF) analysis. We present evidence for both local atomic displacements (local polarization) and for medium-range ($\sim$ 5 Å - 50 Å) ordering, called polar nanoregions (PNRs). These medium-range correlations are modeled using rhombohedral symmetry, enabling for the first time an estimate of the temperature dependence of the volume fraction of the PNRs. This fraction increases with decreasing temperature, reaching the three dimensional percolation threshold below T$\sim$200 K, where the PNRs start to overlap. We discuss the implications of these findings on the dielectric properties of PMN.

Evidence for the existence of local polarization in PMN below T_d $\sim$ 620 K, known as the Burns temperature [4], was deduced from optical and strain measurements [3, 9, 10]. The atomic nature of this polarization in PMN was also studied using extended x-ray absorption fine structure (EXAFS) [11, 12] and atomic pair distribution function (PDF) analysis [13, 14]. Nb K-edge EXAFS measurements on PMN suggested a displacement of Nb ions with respect to their oxygen octahedra by about 0.1 Å from room temperature down to 4.5 K. Pb K-edge EXAFS measurements indicated strong static disorder on the Pb sites, but provided no detailed information about static Pb displacements [11]. This is in contrast to neutron PDF measurements on PMN which clearly showed that the Pb ions are off-center with respect to the O_{12} cage by as much as 0.5 Å [13, 14]. In these earlier PDF measurements, however, a complete picture of local structure in PMN was not obtained due to the limited momentum transfer Q and temperature range available. Thus, the nature of PNRs and their volume fraction were not determined.

Our measurements were performed on the NPDF instrument at the Los Alamos Neutron Science Center (LANSCE). Powder diffraction patterns were corrected for background, absorption and multiple scattering, and normalized using a vanadium spectrum to ob-

tain the total scattering structure function $S(Q)$, using the PDFgetN program [15]. The PDF $G(r)$ is obtained from $S(Q)$ via the Fourier transform shown in Eq. 1,

$$G(r) = 4\pi r[\rho(r) - \rho_0] = \frac{2}{\pi}\int_0^{Q_{max}} \mathrm{Q[S(Q) - 1]sinQr\,dQ}, \quad (1)$$

where ρ(r) and ρ_0 are the atomic number and average number densities, respectively. Since $S(Q)$ includes both Bragg and diffuse scattering, the resultant PDF provides short-, medium-, and long-range structural information [16]. This technique has been used to study local atomic structures [17] and correlated atomic motions of atom pairs [18] in many materials.

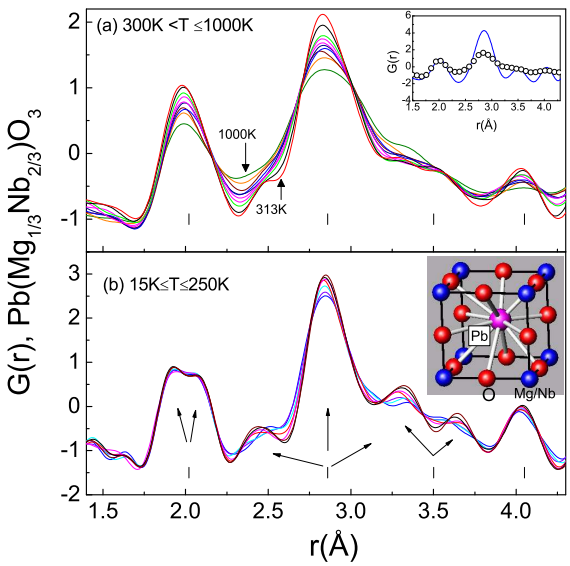

FIG. 1: Temperature evolution of PDF spectra of PMN within a unit cell. (a) High temperature : T=1000 K, 850 K, 750 K, 700 K, 650 K, 600 K, 550 K, 500 K, 400 K, and 313 K, with Q_{max} = 25 Å^{-1}. The inset shows a comparison between an experimental PDF (symbol) and a model PDF (line) at 650 K. See text for details. (b) Low temperature : T=250 K, 220 K, 190 K, 150 K, 100 K, 50 K, and 15 K, with Q_{max} = 30 Å^{-1}. The tick marks indicate (from left to right, respectively) Mg/Nb-O, (Pb-O, O-O), Mg/Nb-Pb, and (Pb-Pb, O-O, Mg/Nb-Mg/Nb) bond lengths in an ideal cubic perovskite structure of PMN. The inset shows the cubic crystal structure with the Pb ion at body center.

We first examine the temperature evolution of the low-r region of the PDF spectra. Fig. 1 (a) shows spectra from 1000 K to 313 K. The tick marks indicate the PDF peak positions for an ideal cubic perovskite structure. The first tick mark represents Mg/Nb-O, the second Pb-O, O-O, the third Mg/Nb-Pb, and the fourth Pb-Pb, O-O, Mg/Nb-Mg/Nb bond lengths. At high temperatures note that the peaks are quite broad and the Pb-Mg/Nb bond is not well defined due to an overlap with the Pb-O bond. As the temperature decreases to room temperature, the Pb-O peak gradually resolves into two peaks at $\sim$ 2.86 Å and 2.5 Å. This splitting indicates a displacement of Pb ions in their O_{12} cages, which breaks 12-fold degeneracy of Pb-O bond distance (see the inset of Fig 1(b)).

In order to understand the origin of these phenomena we compared the experimental PDF at 650 K with a model PDF at the same temperature (shown in the inset of Fig. 1 (a)). In the model PDF we assumed no static displacements and calculated the widths using thermal parameters for Pb, Mg/Nb and O ions obtained from our Rietveld refinement at 650 K. Since the area of the Pb-O peak should be conserved, the comparison shown in the inset to Fig. 1 indicates that the Pb-O peak is much broader in the experiment than in the model, implying that significant static Pb local displacement exists already at 650 K. Thus, the gradual splitting of the Pb-O peak at lower temperatures is mainly due to a decrease of thermal vibrations. Static Pb displacements in PMN above the Burns temperature have also been deduced from Raman measurements [19].

Below room temperature (Fig. 1 (b)) the experimental PDFs reveal more interesting structure. First, the Mg/Nb-O peak around 2.02 Å splits into two peaks, suggesting local Mg/Nb displacements along the $\langle 111\rangle$ direction. Note that this peak shows almost no temperature dependence between 250 K and 15 K, consistent with Nb K-edge EXAFS measurements [11]. In general, PDF peaks become sharper with decreasing temperature due to decreasing thermal motion. Thus, this unusual temperature dependence indicates an increasing distribution of static Mg/Nb displacements with decreasing temperature. Second, the Pb-O peak around 2.85 Å splits into three peaks at $\sim$ 2.45 Å, 2.85 Å, and 3.33 Å. Third, the Pb-Mg/Nb peak around 3.5 Å splits into two Pb-Mg/Nb bonds at $\sim$ 3.33 Å and 3.64 Å mostly due to the displacement of Pb ions. Thus, the peak around 3.3 Å has both Pb-O and Pb-Mg/Nb components. The splitting of the Pb-O and Pb-Mg/Nb peaks below room temperature suggests that the Pb ions may locally shift mostly along $\langle 100\rangle$ or $\langle 111\rangle$ directions. Interestingly, the peak around 4.05 Å (lattice constant of PMN) is well defined; thus, the overall cubic symmetry is maintained although the local cubic symmetry is not.

We now address the medium-range correlations (PNRs) between these local atomic displacements. Fig. 2 (a) shows the PDF spectra from 1000 K to 15 K in the r-range up to 16 Å, and Fig. 2 (b) shows the temperature dependence of the peak intensities in the doublet between 8.0 Å $< r <$9.8 Å. Here both peaks have contributions from almost all possible ionic pairs. The solid line is the calculated temperature dependence of the peak height using the average Pb, Mg/Nb, and O thermal parameters from Bonneau *et al.* [20], which are reproduced in the inset. Note the strong deviation of the data below

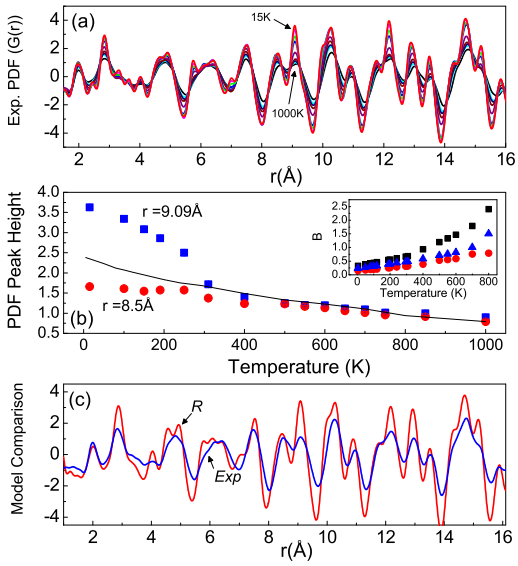

FIG. 2: (a) Temperature dependence of the PDF spectra of PMN at temperatures T=1000 K, 750 K, 650 K, 500 K, 313 K, 250 K, 190 K, 100 K, 15 K. All PDFs were obtained with Q_{max}=25Å^{-1}. (b) PDF peak height in the doublet between 8.0 Å $< r <$9.8 Å as a function of temperature. The line is the expected average PDF peak height using the thermal parameters in the inset. The inset shows the thermal parameters of Pb (square), Mg/Nb (circle) and O (triangle) [20]. (c) Comparison of rhombohedral (R-model) PDF with the experimental PDF at 650 K. *R* and *Exp* represent the R-model and experimental (paraelectric cubic) PDFs, respectively.

T∼250 K, an indication of PNRs, as we now show.

We modeled the PNRs using rhombohedral symmetry (R-model: space group R3m), wherein the Pb, Mg/Nb and oxygen octahedra are displaced along the ⟨111⟩ directions, assuming rigid oxygen octahedra. Similar models of rhombohedral correlations with ⟨111⟩ atomic displacements [21, 22, 23] and non-collinear ⟨100⟩ displacements that average to rhombohedral symmetry [24] have been proposed in $Pb(Mg_{1/3}Nb_{2/3})O_3$ and $Pb(Sc_{1/2}Ta_{1/2})O_3$, respectively. Attempts to model our data using displacements of orthorhombic symmetry (with the atoms and oxygen octahedra displaced along ⟨110⟩ directions with the same magnitudes as in the rhombohedral model) were unsuccessful, with some PDF peaks being too strong and others too weak.

In Fig. 2 (c) we compare the R-model PDF with the experimental PDF at 650 K. For the R-model PDF calculation the thermal parameters were taken from Bonneau *et al.* [20], and the following atomic positions were used, determined to best simulate the differences between low temperature PDFs and the PDF at 650 K: Pb (-0.0392, -0.0392, -0.0392), Mg/Nb (0.5062, 0.5062, 0.5062) and O (0.5308, 0.5308, 0.0308).

The PDF peaks of the R-phase are quite distinct from those of the paraelectric cubic phase. In fact, the relative intensities of the PDF peaks in the R-phase and in the paraelectric cubic phase resemble the low-temperature and high-temperature end members shown in Fig. 2 (a), respectively. Therefore, if we assume that PNRs are dispersed as "islands" in the paraelectric cubic lattice [21], growing in size and volume fraction with decreasing temperature, we expect that features of the R-model PDF will become more evident with decreasing temperature. This is exactly what we observe in the experimental PDFs shown in Fig. 2 (a).

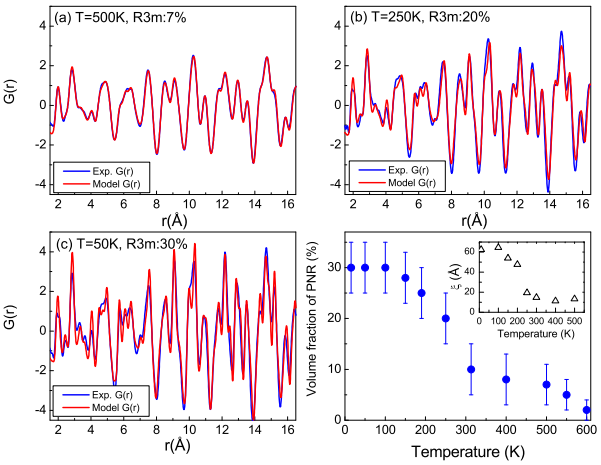

FIG. 3: Comparison of the "two-phase" model PDF with the experimental PDFs at (a) T=500 K, (b) T=250 K, (c) T=15 K. The model PDF is calculated from $G_m = \alpha(T)G_R+(1-\alpha(T))G_C$, where G_R and G_C are model PDFs for the rhombohedral and paraelectric phases. $\alpha(T)$ is the volume fraction of the rhombohedral phase. (d) The volume fraction increases with decreasing temperature, reaching 30% at 15K. The inset shows the correlation length of local polarization as a function of the temperature (taken from Xu *et al.* [25]).

The volume fraction of the PNRs was estimated using a simple model PDF: $G_m = \alpha(T)G_R+(1-\alpha(T))G_C$, where G_R and G_C are rhombohedral and paraelectric cubic model PDFs, respectively, and $\alpha(T)$ is the volume fraction of the rhombohedral phase as a function of temperature. For the R-model PDF calculations the atomic coordinates given above were used for all temperatures. For the paraelectric cubic phase, we first introduced static displacements of ions in a $10 \times 10 \times 10$ unit cell via a reverse Monte-Carlo (RMC) fit to the the experimental PDF at 650 K, using the DISCUS program [26]. These static displacements were then fixed, and the cubic model PDF was calculated at various temperatures using the thermal parameters from Bonneau *et al.* [20]. (The same thermal parameters are used for both cubic and rhombohedral phases.) After calculating both para-

electric cubic and rhombohedral PDFs at a given temperature, α(T) was adjusted to obtain the best match to the corresponding experimental PDF. Figures 3 (a-c) show these comparisons at 500 K, 250 K, and 50 K in the r-range up to r=16 Å. Considering the simplicity of the model PDF calculations, the overall agreement at various temperatures is very good.

In Fig. 3(d) we show the temperature dependence of α(T), along with the correlation length of local polarization determined by Xu *et al.* using neutron elastic diffuse scattering [25], shown in the inset. The volume fraction steadily increases with decreasing temperature, reaching $\sim$ 30% at 15 K. The correlation length ξ of local polarization increases from $\xi \sim$ 15 Å to $\xi \sim$ 60 Å. Note that around T$\sim$200 K, where the correlation length drastically increases, α(T) reaches the percolation threshold $P_c\sim$28% for spherical objects in three dimensions [27]. This implies that the PNRs start to overlap with each other below T$\sim$200 K. This correlates well with the abrupt increase in the correlation length of local polarization to $\xi \sim$ 50 - 60 Å, determined independently.

Neutron scattering measurements by Wakimoto *et al.* [28] suggest that locally, each PNR maintains a stable spontaneous polarization below T$\sim$220 K where the correlation length is about $\sim$ 50-60 Å. Further growth of these large PNRs (beyond $\sim$ 60 Å) may be hindered by electric and elastic energy barriers, which are proportional to the size of the PNR. In an applied electric field, however, the polarizations in the separate PNRs are aligned, and the separate PNRs form a macro polar domain. Once the macro polar domain is formed, the dipoles in the domain do not randomly orient even after the electric field is turned off.

This picture helps to explain some basic behavior found in PMN, such as hysteresis in the field-induced polarization [29], the field-induced rhombohedral phase transition below 220 K [30] and the anomaly in the dielectric permittivity near 212 K upon field heating after zero-field cooling [7]. Our measurements, therefore, provide direct local structural evidence for the importance of percolating PNRs in explaining many features of the relaxor behavior found in PMN below the Burns temperature.

Work at Los Alamos was carried out under the auspices of the US DOE/Office of Science. This work has benefited from the use of NPDF at the Lujan Center at Los Alamos Neutron Science Center, funded by DOE Office of Basic Energy Sciences and Los Alamos National Laboratory funded by Department of Energy under contract W-7405-ENG-36. The upgrade of NPDF has been funded by NSF through grant DMR 00-76488.

* Electronic address: jeong@lanl.gov

[1] G. A. Smolenskii and A. I. Agranovskaya, Sov. Phys. Tech. Phys., Engl. Transl. **3**, 1380 (1958).
[2] K. Binder and A. P. Young, Rev. Mod. Phys. **58**, 801 (1986).
[3] L. E. Cross, Ferroelectrics **76**, 241 (1987).
[4] G. A. Samara, J. Phys: Condens. Matter **15**, R367 (2003).
[5] D. Viehland, J. F. Li, S. J. Jang, L. E. Cross, and M. Wuttig, Phys. Rev. B **43**, 8316 (1991).
[6] E. V. Colla, E. Y. Koroleva, N. M. Okuneva, and S. B. Vakhrushev, Phys. Rev. Lett. **74**, 1681 (1995).
[7] V. Westphal, W. Kleemann, and M. D. Glinchuk, Phys. Rev. Lett. **68**, 847 (1992).
[8] H. You and Q. M. Zhang, Phys. Rev. Lett. **79**, 3950 (1997).
[9] G. Burns and F. H. Dacol, Solid State Commun. **48**, 853 (1983).
[10] J. Zhao, A. E. Glazounov, Q. M. Zhang, and B. Toby, Appl. Phys. Lett. **72**, 1048 (1998).
[11] E. Prouzet, E. Husson, N. de Mathan, and A. Morell, J. Phys: Condens. Matter **5**, 4489 (1993).
[12] I.-W. Chen, P. Li, and Y. Wang, J. Phys. Chem. Solids **57**, 1525 (1996).
[13] T. Egami, H. Rosenfeld, B. Toby, and A. Bhalla, Ferroelectrics **120**, 11 (1991).
[14] H. D. Rosenfeld and T. Egami, Ferroelectrics **150**, 183 (1993).
[15] Th. Proffen and S. J. L. Billinge, Jour. Appl. Cryst. **32**, 572 (1999).
[16] T. Egami and S. J. L. Billinge, *Underneath the Bragg Peaks: Structural Analysis of Complex Materials* (Pergamon Press, Oxfore, UK, 2003).
[17] I.-K. Jeong, F. Mohiuddin-Jacobs, V. Petkov, S. J. L. Billinge, and S. Kycia, Phys. Rev. B **63**, 205202 (2001).
[18] I.-K. Jeong, Th. Proffen, F. Mohiuddin-Jacobs, and S. J. L. Billinge, J. Phys. Chem. A **103**, 921 (1999).
[19] I. G. Siny and T. A. Smirnova, Ferroelectrics **90**, 191 (1989).
[20] P. Bonneau, P. Garnier, G. Calvarin, E. Husson, J. R. Cavarri, A. W. Hewat, and A. Morrel, J. Solid State Chem. **91**, 350 (1991).
[21] N. de Mathan, E. Husson, G. Calvarin, J. R. Gavarri, A. W. Hewat, and A. Morell, J. Phys: Condens. Matter **3**, 8159 (1991).
[22] N. Takesue, Y. Fujii, and H. You, Phys. Rev. B **64**, 184112 (2001).
[23] R. Blinc, V. Laguta, and B. Zalar, Phys. Rev. Lett. **91**, 247601 (2003).
[24] W. Dmowski, M. K. Akbas, P. K. Davies, and T. Egami, J. Phys. Chem. Solids **61**, 229 (2000).
[25] G. Xu, G. Shirane, J. R. D. Copley, and P. M. Gehring, Phys. Rev. B **69**, 064112 (2004).
[26] Th. Proffen and R. Neder, Jour. Appl. Cryst. **30**, 171 (1997).
[27] E. J. Garboczi, K. A. Snyder, J. F. Douglas, and M. F. Thorpe, Phys. Rev. E **52**, 819 (1995).
[28] S. Wakimoto, C. Stock, R. J. Birgeneau, Z.-G. Ye, W. Chen, W. J. L. Buyers, P. M. Gehring, and G. Shirane, Phys. Rev. B **65**, 172105 (2002).
[29] V. A. Bokov and I. E. Myl'nikova, Soviet Physics-Solid State **3**, 613 (1961).
[30] G. Calvarin, E. Husson, and Z. G. Ye, Ferroelectrics **165**, 349 (1995).